ACS APPLIED MATERIALS & INTERFACES

Research Article

www.acsami.org

Rapid Removal of Hg(II) from Aqueous Solutions Using Thiol-Functionalized Zn-Doped Biomagnetite Particles

Feng He,*[,†] Wei Wang,[†] Ji-Won Moon,[‡] Jane Howe,[3] Eric M. Pierce,[†] and Liyuan Liang[†]

[†]Environmental Sciences Division, [‡]Biosciences Division, and [3]Materials Science & Technology Division, Oak Ridge National Laboratory, Oak Ridge, Tennessee 37831, United States

Supporting Information

ABSTRACT: The surfaces of Zn-doped biomagnetite nanostructured particles were functionalized with (3-mercaptopropyl)trimethoxysilane (MPTMS) and used as a high-capacity and collectable adsorbent for the removal of Hg(II) from water. Fourier transform infrared spectroscopy (FTIR) confirmed the attachment of MPTMS on the particle surface. The crystallite size of the Zn-doped biomagnetite was ~17 nm, and the thickness of the MPTMS coating was ~5 nm. Scanning transmission electron microscopy and dynamic light scattering analyses revealed that the particles formed aggregates in aqueous solution with an average hydrodynamic size of 826 ± 32 nm. Elemental analyses indicate that the chemical composition of the biomagnetite is $Zn_{0.46}Fe_{2.54}O_4$, and the loading of sulfur is 3.6 mmol/g. The MPTMS-modified biomagnetite has a calculated saturation magnetization of 37.9 emu/g and can be separated from water within a minute using a magnet. Sorption of Hg(II) to the nanostructured particles was much faster than other commercial sorbents, and the Hg(II) sorption isotherm in an industrial wastewater follows the Langmuir model with a maximum capacity of ~416 mg/g, indicating two −SH groups bonded to one Hg. This new Hg(II) sorbent was stable in a range of solutions, from contaminated water to 0.5 M acid solutions, with low leaching of Fe, Zn, Si, and S (<10%).

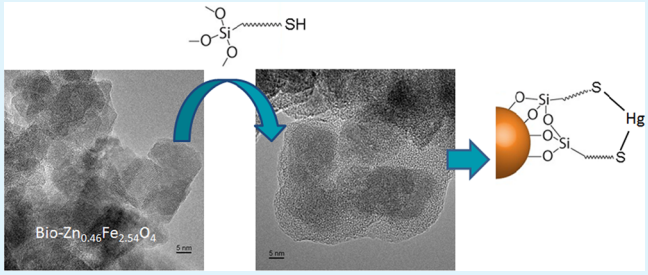

KEYWORDS: *Zn-doped biomagnetite, nanoparticles, (3-mercaptopropyl)trimethoxysilane (MPTMS), superparamagnetic, mercury sorption, stability*

INTRODUCTION

Mercury (Hg), in particular Hg(II) in water, presents a serious environmental concern, because of its transformation to the potent neurotoxin methylmercury, which can be bioaccumulated and biomagnified in aquatic food chains.[1−3] To protect ecosystems, the discharge of mercury into aquatic systems often falls below strict regulatory limits that are much lower than the maximum concentration level of Hg (2 μg/L) regulated by the U.S. Environmental Protection Agency (EPA) for drinking water. For example, at the Y-12 National Security Complex (NSC) in Oak Ridge, TN, the interim level of mercury for effluent discharge to the receptor (East Fork Poplar Creek) is 200 ng/L and the future goal is to meet the ambient water quality criteria for mercury in Tennessee (51 ng/L). Currently, the precipitation/coprecipitation (e.g., with sulfide ions) methods that are the most commonly used processes to treat Hg(II) contaminated water are not able to reduce the concentrations of mercury to acceptable limits.[4,5]

In response to these challenges, a variety of materials has been developed and tested for removing low levels of Hg(II) from contaminated waters. Traditional adsorbents such as activated carbon,[6,7] low-cost natural biosorbents such as chitosan,[8,9] natural inorganic ion-exchange materials such as zeolites,[10] clay,[11] peat,[12] bentonite,[13] and others[14] suffer from low selectivity, low capacity, and weak binding affinity for mercury. Recent research has focused on development of thiol-functionalized adsorbents to improve the selectivity for Hg(II), including functionalized clays,[15−17] resins,[7,18] organoceramics,[19,20] mesoporous silicates,[21−28] and mesoporous carbon.[29] The thiol-functionalized materials are selective and have a strong binding affinity for Hg^{2+}, as a consequence of a soft Lewis acid−base interaction.[30]

Unfortunately, the efficiency of thiol-based porous sorbents, such as resins, is impeded by diffusion processes, which limit mercury transport to the adsorption sites (i.e., thiol groups). For microscale mesoporous sorbents (e.g., thiol SAMMS), pore diffusion is improved but the separation of the used materials from water remains problematic. Therefore, a dispersible and recoverable sorbent with highly accessible sorption sites is desired for the removal of Hg(II) from aqueous solutions. Superparamagnetic magnetite nanostructured particles are this type of material. With primary particle sizes of <25 nm, magnetite nanostructured particles offer a large surface area, in addition to superparamagnetic properties. They are attracted to a magnetic field but do not retain magnetic properties when the

Received: June 7, 2012
Accepted: August 1, 2012
Published: August 1, 2012

   dx.doi.org/10.1021/am301031g | ACS Appl. Mater. Interfaces 2012, 4, 4373−4379

field is removed, making them highly useful in novel separation processes.[31]

Superparamagnetic particles, with or without surface functionalization, have been reported to successfully capture Cr(VI),[32] As(V),[33,34] Cd(II),[35] Cu(II),[36,37] Pb(II),[31] and Hg(II).[31,38,39] Surface modification of magnetite nanostructured particles with dimercaptosuccinic acid,[31] humic acid,[39] poly(3,4-ethylenedioxythiophene),[40] 1,5-diphenylcarbazide,[41] and vinylpyrrolidone[42] has been performed to remove Hg(II) particularly from aqueous solutions. Surface modification of magnetic silica particles with mercaptopropyl-trimethoxysilane,[38,43] quaternary ammonium,[44] and 1,4-bis(triethoxysilyl)-propane tetrasulfide[45] has also been reported. Not surprisingly, surface modification of magnetite nanostructured particles with thiol groups showed the most-enhanced Hg(II) removal efficiency and highest adsorption capacity.[31]

Chemically synthesized magnetite or silica-coated magnetite nanostructured particles were typically used in prior studies.[31,38−45] Here, we describe a thiol-functionalized Zn-doped biomagnetite nanostructured material for Hg(II) removal. The Zn-doped biomagnetite was synthesized using *nanofermentation* methods. The synthesis details are given in refs 46−48. The nanofermentation method has several advantages, including low energy input (close to room temperature to 65 °C), good scalability and reproducibility (e.g., 13.1 ± 0.8 nm of Zn-doped biomagnetite from continuous running of seven batches of 30-L reactors), an environmentally friendly process that does not require genetic manipulation or toxic organic solvents, and low cost, requiring only sugar as nutrients and inexpensive metal salts as precursors.[47] In addition, the novelty of our approach includes the doping of low-level Zn to enhance the magnetism of the nanostructured materials and the direct coating of thiol ligands on biomagnetite surfaces through robust Si−O−Fe bonding. To the best of our knowledge, this is the first time that biosynthesized, transition-metal-doped, nanostructured magnetite has been employed in an environmental application. Accordingly, we carefully evaluated the stability of the doped biomagnetite in environmental media.

MATERIALS AND METHODS

Materials. All chemicals used in the experiments were either ACS reagent grade or better. Hg(II) solutions were prepared from a $Hg(NO_3)_2$ solution (0.1 M). Granular activated carbon (F300) from Calgon Carbon was used as a base sorbent. Granular thiol SAMMS was obtained from Steward Advanced Materials, Inc. Thiol-based resins GT-74, XUS 43604, Keylex, and SIR-200 were obtained from Rohm and Haas, Dow, SolmeteX, and ResinTech, respectively.

Synthesis of the Nanostructured Biomagnetite. Synthesis of Zn-doped biomagnetite was performed following the methods provided in ref 46−48 and briefly described in the Supporting Information (SI).

Surface Modification of the Biomagnetite. A known amount of Zn-doped biomagnetite particles was first dispersed into a mixture of 200 mL of ethanol and 10 mL of H_2O to produce a suspension, followed by adding 2 mL of (3-mercaptopropyl)trimethoxysilane (MPTMS) (Alfa Aesar, 95%) drop by drop while stirring. After being reacted for 6 h, the pH of the reaction mixture was adjusted to ∼9.5 by $NH_3{\cdot}H_2O$ and continuously reacted for an additional 24 h. The functionalized Zn-doped biomagnetite was then collected by a 1.3T neodymium iron boron (NdFeB) magnet (K&J Magnetic, Inc.) and washed with deionized (DI) water until pH ∼7 was attained.

Characterization of the Nanostructured Materials. Scanning transmission electron microscopy (STEM) was carried out using a Hitachi Model HF-3300 TEM/STEM system at 300 keV. Energy-dispersive X-ray spectroscopy (EDS) was performed, using a Bruker solid-state detector attached to the microscope, and analyzed using the Bruker's Espirit 1.9 software. The HF-3300 system has a secondary electron (SE) detector that enables the recording of both transmitted electron (TE) and SE images. The crystalline structure of the Zn-doped biomagnetite was examined using X-ray diffractometry (XRD) (Model PAD V, Scintag, Inc., Sunnyvale, CA) equipped with Cu Kα radiation at 45 kV/40 mA, with a scan rate of 2°−3° 2θ/min. The average crystallite size was derived from XRD results using the Scherrer equation.[49] Infrared spectra were recorded in the 4000−400 cm^{-1} range, using a Nicolet Magna-760 FTIR spectrometer by dispersing the powder samples in KBr pellets. Average hydrodynamic sizes and zeta potentials of the particles in water suspensions were determined by a dynamic light scattering (DLS) method (Brookhaven Instruments, Model 90Plus/MI-MAS, Holtsville, NY). Surface areas of the samples were measured by a Gemini VII 2390 Surface Area Analyzer (Micromeritics, Norcross, GA) and a FlowPrep 060 sample degas system using the Brunauer−Emmett−Tuller (BET) N_2 adsorption method. Determination of the elemental composition of the thiol-functionalized Zn-doped biomagnetite was performed by dissolving 10 mg freeze-dried particles in 5 mL of HNO_3 (15.6 M). The samples were then diluted in 2% HNO_3 and subjected to analysis for Fe, Zn, Si, and S using inductively coupled plasma−optical emission spectroscopy (ICP-OES) (IRIS Intrepid II, Thermo Scientific, USA).

Hg(II) Sorption Kinetics and Partitioning Coefficient (K_d). Hg(II) solutions prepared with deionized water and Y-12 wastewater (YWW) were used as test solutions to evaluate performance of the biomagnetite-based mercury sorbents. Stock solution of 0.1 M $Hg(NO_3)_2$ was used to prepare a 10 μM Hg(II) solution in DI water. The YWW solution was collected from a source area at Y-12 NSC, filtered through a 0.45-μm filter, and the filtrate Hg(II) was measured to be 0.12 μM Hg(II). Additional water chemistry details of the YWW solution are provided in Table S1 in the Supporting Information. Mercury sorption onto the biomagnetite was performed by adding the sorbents to the Hg(II) solutions. For DI water kinetics tests, the liquid:solid ratio (L/S) was 10 000 mL/g; however, for the wastewater tests, the L/S was decreased to 3000 mL/g (i.e., the amount of the sorbents was tripled). The testing solution volume was 100 mL. The pH of the starting solution was 7.0 ± 0.1 for Hg(II) in DI water and 8.0 ± 0.1 for the wastewater. The reactors were shaken at room temperature (22 ± 1 °C) for up to 19 h. From each reactor, a 1.5-mL aliquot of the well-mixed slurry was sampled at designated intervals, and the particles were separated out of the solution immediately using a 1.3T NdFeB magnet. An aliquot of the solution (1 mL) was then preserved with BrCl (1%) and analyzed for total mercury concentration. Mercury was analyzed using a RA-915+ mercury spectrometer (Lumex, Twinsburg, OH) with a detection limit of 25 pg.

For comparison, sorption kinetics of commercial thiol chelating sorbents were run in parallel to remove Hg(II) from YWW. For those experiments, the L/S ratio was 3000 mL/g and the sorption time was 19 h. The sorbents in sampled aliquots were removed using an Acrodisc syringe filter (0.2 μm Supor membrane) for aqueous Hg(II) analysis. The partitioning coefficient for the sorption of Hg(II), K_d (in mL/g), was calculated as the ratio of the amount of Hg(II) sorbed (as mg/g dry sorbents) divided by the concentration of Hg(II) remaining in the equilibrium solution (as mg/mL), i.e.,

$$K_d = \frac{\text{Hg(II) sorbed on sorbents (mg/g)}}{\text{Hg(II) in solution (mg/mL)}}$$

Sorption Isotherm. Batch isotherm tests were carried out for selected sorbents in 120-mL amber glass bottles with Teflon-lined screw caps. The tests were initiated by adding 0.01 g (dry weight) of a sorbent to 100 mL of a Y-12 wastewater spiked with Hg(II) at initial concentration of 0.04−50 mg/L. The mixture was then shaken on an orbital shaker for 5 days to ensure the sorption equilibrium was reached. We note that no precipitation of $Hg(OH)_2$ was observed during the isotherm tests. The mercury remaining in the solution was then analyzed and the mercury uptake (q_e) was calculated. The

equilibrium data were fitted using the Langmuir sorption model, which is given by

$$q_e = \frac{q_{max} K_L C_e}{1 + K_L C_e}$$

where q_{max} is the sorption capacity of the sorbent (in units of mg Hg(II)/g sorbent), C_e the equilibrium concentration of Hg(II), and K_L the Langmuir constant (in units of L solution/mg Hg(II)) representing the energy of sorption.

Stability of Thiol-Functionalized Zn-Doped Biomagnetite. Stability of the nanostructured materials in solution was evaluated using the Y-12 wastewater and HNO_3/NaOH solution at various concentrations. After 6 h of contact time, an aliquot of the leachate from 100 mg/L suspension was collected and analyzed for Fe and Zn, using inductively coupled plasma–mass spectroscopy (ICP-MS) (Model Elan6100, Perkin–Elmer, USA), and for Si and S, using ICP-OES (Model IRIS Intrepid II, Thermo Scientific, USA).

RESULTS AND DISCUSSION

Characterization of the Nanostructured Biomagnetite. Surface modification with MPTMS moieties on the Zn-doped biomagnetite was successful, as shown by infrared spectroscopic analysis of the material in Figure 1a. We term this newly synthesized Hg(II) sorbent material MPTMS-biomagnetite. In the IR spectrum, stretching bands attributed to the S–H and C–S vibrations at 2546 and 690 cm^{-1}, respectively, and C–H vibrations in the 2850–2930 and 1250–1500 cm^{-1} regions were observed. Stretching bands assigned to Si–C and Si–O–M (M = Si, Fe, or Zn) at 1105 and 1034 cm^{-1}, respectively,[15] were also detected. The FTIR results confirm that MPTMS interacts with the biomagnetite surface forming a robust coating. Scheme S1 in the Supporting Information provides a conceptual illustration of the formation of MPTMS-biomagnetite.

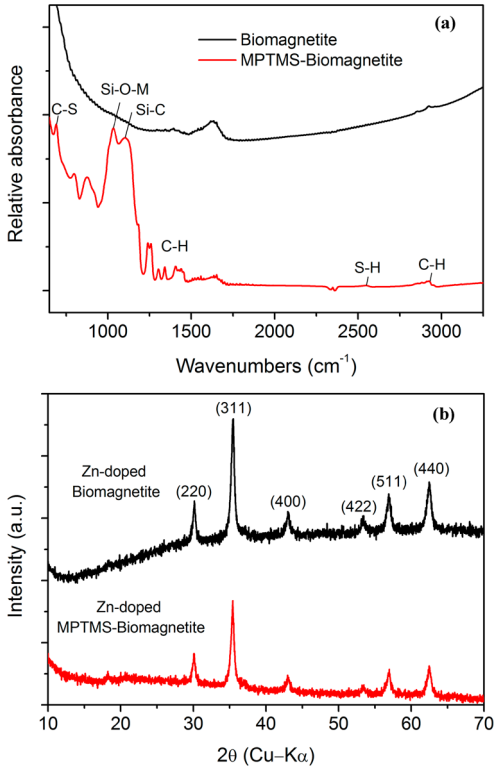

Figure 1. (a) Infrared (IR) spectrum and (b) XRD pattern of Zn-doped biomagnetite with and without thiol functionalization.

The powder XRD patterns of biomagnetite and MPTMS-biomagnetite are shown in Figure 1b. The biomagnetite has a clear magnetite pattern, indicating that incorporation of a low percentage of Zn did not change the magnetite crystalline structure. The similar XRD patterns for biomagnetite and MPTMS-biomagnetite further indicate that the surface coating did not affect the biomagnetite crystalline structure. The crystalline size of MPTMS-biomagnetite (i.e., 16.7 ± 0.4 nm) is well below the superparamagnetic size of 20–35 nm.[50] Since the Zn-doped biomagnetite is superparamagnetic, based on previous measurements, using a superconducting quantum interference device (SQUID),[48,51] as well as the fact that the MPTMS coating is unlikely to alter its superparamagnetic properties,[52,53] the MPTMS-biomagnetite is also considered to be superparamagnetic. Figure 2 shows representative high-resolution TEM images of the Zn-doped biomagnetite (Figure 2a) and MPTMS-biomagnetite (Figure 2b). Figure 2b clearly shows an amorphous layer (i.e., MPTMS) ~5 nm thick on the biomagnetite for MPTMS-biomagnetite particles. The primary MPTMS-biomagnetite particle size is ~15–18 nm, which is consistent with the XRD measurement. However, the primary particles aggregated together through the MPTMS coating and formed large clusters, as shown in the STEM image (Figure 3). DLS measurement further showed that an average hydrodynamic size of the MPTMS-biomagnetite aggregates is 826 ± 32 nm. BET measurement showed that the surface area of MPTMS-biomagnetite is 17.4 m^2/g, compared to 75.6 m^2/g of uncoated biomagnetite, indicating the significant aggregation of MPTMS-biomagnetite particles bridged by MPTMS.

The zeta potentials of the as-prepared biomagnetite and MPTMS-biomagnetite were measured at varied pH values. The isoelectric point (IEP) of biomagnetite was pH ~5.6, which is close to that reported for chemically synthesized Fe_3O_4 nanoparticles.[39] Therefore, the doping of Zn in Fe_3O_4 through the biofermentation method did not significantly affect the surface charge of the magnetite. However, the IEP of MPTMS-biomagnetite decreased to 2.3, which is unexpected with the coating of uncharged MPTMS. One possible explanation is that some of the –SH on the particle surface may have been oxidized to $-SO_3^-$, which made the particle surface negatively charged, even at low pH. An oxidized S peak was observed in X-ray photoelectron spectroscopy (XPS) analysis of SiO_2 surface modified with MPTMS.[54] However, the content of $-SO_3^-$ groups (strong acid) should be fairly low, because the pH of MPTMS-biomagnetite (100 mg/L) in 0.1 M NaCl solution was ~7.5 (no acidity).

Elemental analysis of Si, Zn, Fe, and S indicated that 1 g of the MPTMS-biomagnetite contained 0.42 ± 0.03 g of $Zn_{0.46}Fe_{2.54}O_4$ and 0.57 ± 0.01 g of MPTMS (or 3.6 mmol of S). The almost perfect mass balance, assuming that all of the sulfur is present as –SH in MPTMS-biomagnetite, further indicates that the oxidation of –SH to $-SO_3^-$ was not significant. Assuming that the density of the MPTMS layer on biomagentite is the same as its bulky density, a 5-nm layer coverage would contain 19.8 wt % MPTMS and 80.2 wt % $Zn_{0.46}Fe_{2.54}O_4$. Thus, the observed value of 57 wt % MPTMS suggests that the precipitation/polymerization of MPTMS on biomagnetite particles is not even. The STEM elemental mapping results (Figure 3) visualize not only the deposition of MPTMS on the biomagnetite surface but also its significant self-polymerization resulting in spherical silica particles. This is

dx.doi.org/10.1021/am301031g | ACS Appl. Mater. Interfaces 2012, 4, 4373–4379

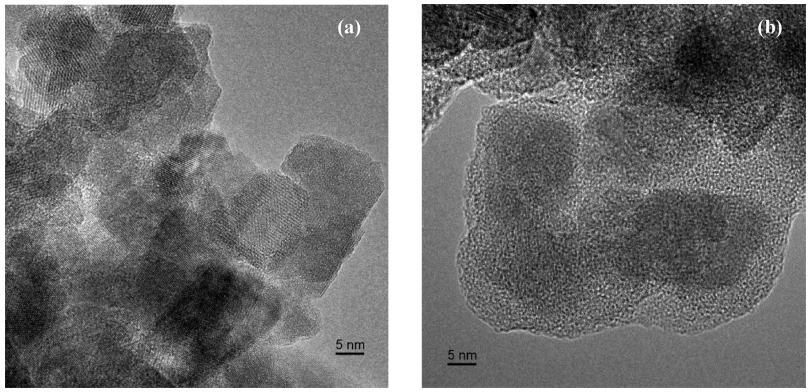

Figure 2. High-resolution TEM images of (a) Zn-doped biomagnetite and (b) MPTMS-biomagnetite. Scale bar is 5 nm.

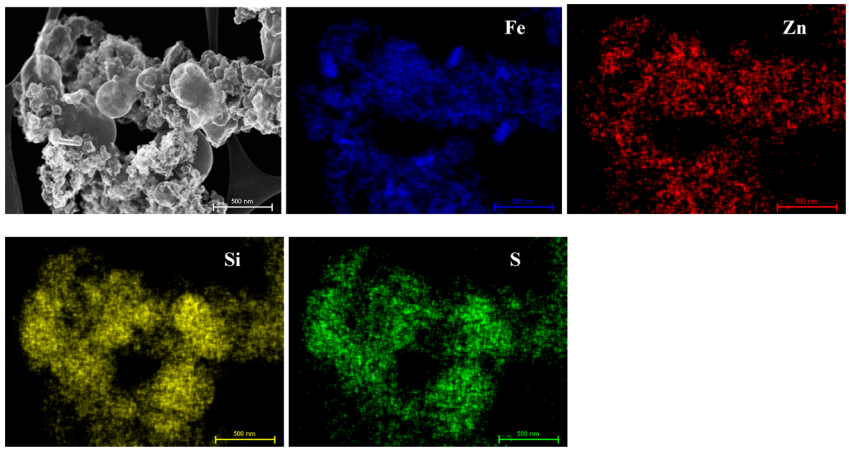

Figure 3. Secondary-electron image of the MPTMS-biomagnetite and X-ray maps of Fe, Zn, Si, and S. Scale bar is 500 nm.

Table 1. Comparison of Important Features of Biomagnetite-MPTMS and Its Hg(II) Uptake Performance with Other Reported Magnetic Nanostructured Mercury Sorbents

magnetic core	functionalized groups	saturation magnetization (emu/g)	solution matrix	pH	Hg(II) capacity (mg/g)	ref(s)
Fe_3O_4	thiol	53.8	groundwater	8.1	227	31, 56
Fe_3O_4	humic acid	68.1	DI water	6	97.7	39
Fe_3O_4/SiO_2	quaternary ammonium	6.02	DI water	5.5	19.6	44
Fe_3O_4/SiO_2	thiol	6.87	DI water	N/A	256	38
Fe_3O_4/SiO_2	sulfide	11.7	DI water	N/A	N/A	45
Fe_3O_4	thiol/amine	N/A	DI water	7.5−10	280	42
biomagnetite	thiol	37.9	wastewater	8	416	this work

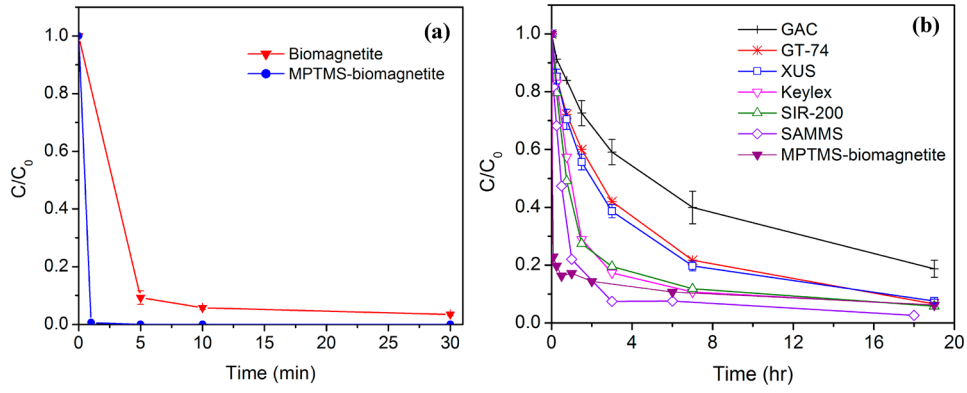

Figure 4. (a) Kinetics of sorption of 10 μM Hg(II) (pH 7.0, L/S = 10 000) from DI water by biomagnetite and MPTMS-biomagnetite, and (b) kinetics of sorption of 0.12 μM Hg(II) (pH 8.0, L/S = 3000) from YWW water by MPTMS-biomagnetite, compared with other commercial sorbents.

not surprising, given that hydrolyzed MPTMS not only dehydrates with hydroxyl groups on the metal oxide surface but can also undergo self-polymerization to form a polymer.[55] The extent of self-polymerization depends on the MPTMS concentration and water content. The relatively high MPTMS concentration (0.05 M), and the high content of water in our system, favored self-polymerization of MPTMS either on the surface of biomagnetite or by forming separate particles. We note that the spherical particles are physically attached to the biomagnetite through Si−O−Si bonds and are able to be utilized for Hg(II) capture.

The saturation magnetization of the Zn-doped biomagnetite was measured to be 90.3 emu/g.[48] Based on this, and with the content of 42% $Zn_{0.46}Fe_{2.54}O_4$ in MPTMS-biomagnetite, the saturation magnetization of MPTMS-biomagnetite was calculated to be 37.9 emu/g, which is relatively high, compared to reported values of other magnetic nanostructured particles functionalized for Hg(II) removal, as shown in Table 1. The high magnetism of the particles allows their rapid separation from water. At an L/S ratio of 10^4, only 1% of the biomagnetite were left in the solution after 1 min of magnetic separation. The efficiency of the magnetic removal was as effective as centrifugation, which removes 99% of the biomagnetite from the solution at 1380 rcf in 15 min.

Sorption Kinetics and K_d. The rate of the sorption reaction can be used to determine the residence time required to remove metal ions such as Hg(II). Rapid sorption will minimize the residence time in the reactor and, therefore, the size of the reactor. Figure 4a compares the uptake rate of Hg(II) from DI water at pH 7 by biomagnetite and MPTMS-biomagnetite. After 1 min of contact time, 99.3% of 2 mg/L of Hg(II) was removed by MPTMS-biomagnetite, while only 80% of Hg(II) was removed by biomagnetite. At neutral pH, the surfaces of biomagnetite and biomagnetite-MPTMS are both negatively charged while the Hg(II) is mainly present as $Hg(OH)_2$. Therefore, electrostatic attraction should not be the main mechanism causing the rapid adsorption of mercury by MPTMS-biomagnetite. Instead, it can be attributed to the high affinity between −SH groups and Hg^{2+}, as well as to the readily available −SH groups at the nanostructured material surface.

The uptake of Hg(II) from YWW by MPTMS-biomagnetite slowed considerably. For example, Hg(II) removal from YWW was ∼77% after 5 min of contact time (see Figure 4b). The hydrodynamic size of the MPTMS-biomagnetite (847 ± 66 nm) did not increase significantly in the slightly higher ionic strength YWW; thus, it is not a primary cause of the slow uptake of Hg(II). This sorption retardation is attributed to the dissolved organic matter (DOC = 2.3 mg/L), as well as other metal ions (see Table S1 in the Supporting Information) in YWW. The competitive complexation of Hg(II) with dissolved organic matter (DOM) limits the interactions between Hg^{2+} and −SH groups on MPTMS-biomagnetite. Other metal ions in the wastewater can also compete with Hg^{2+} for active sorption sites. Nevertheless, compared to the commercial sorbents, MPTMS-biomagnetite removed Hg(II) rapidly. As a comparison, in order to achieve 77% removal of Hg(II), the required contact time was ∼1, 3, 7, and 16 h for SAMMS, SIR 200, GT-74, and granular active carbon (GAC), respectively. Commercial resins such as SIR-200, GT-74, and GAC are porous materials, and could suffer from slow diffusion of Hg(II) into the sorption sites inside the pores. Thiol SAMMS was designed with an open pore structure, allowing for rapid diffusion of Hg^{2+} into the −SH binding sites.[25,26] However, the engineering (or aggregation) form of SAMMS used in this study may still suffer from a minor amount of internal diffusion. In contrast, nanostructured MPTMS-biomagnetite has extensive −SH binding sites on the surface. This, combined with limited internal diffusion, resulted in the extremely rapid Hg(II) sorption kinetics. At the same time, the high magnetism of the MPTMS-biomagnetite particles allows the rapid separation of sorbents from the treated water.

The 19-h K_d values of Hg(II) sorption by GAC, GT-74, XUS, Keylex, SIR-200, MPTMS-biomagnetite, and SAMMS are 13 000, 43 000, 37 000, 46 000, 49 000, 46 000, and 111 000 mL/g in YWW solution, respectively. The results show that thiol sorbents are superior to the selected GAC (Calgon F300) for capturing Hg(II). However, the K_d value for thiol resins and MPTMS-biomagnetite did not differ significantly as the reaction approached equilibrium. The SAMMS material has a better Hg(II) selectivity than the other thiol-based sorbents, and thus can decrease Hg(II) to a lower concentration range under the same operating conditions.

Sorption Capacity. Figure 5 shows the adsorption isotherms of Hg(II) on MPTMS-biomagnetite, biomagnetite,

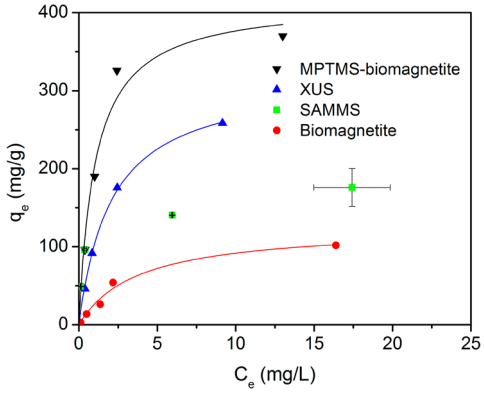

Figure 5. Adsorption isotherm of Hg(II) in the YWW solution by MPTMS-biomagnetite, XUS, SAMMS, and biomagnetite (pH 8.0, L/S = 3 000). Solid lines represent Langmuir model fitting of the data.

SAMMS, and XUS in YWW solution (pH 8.0). XUS is selected as a representative of the thiol-based resins. The data of Hg(II) uptake versus equilibrium Hg(II) concentration show a good fit with a Langmuir adsorption model for MPTMS-biomagnetite, biomagnetite, and XUS, compared to a Freundlich model (see Figure S1 and Table S2 in the Supporting Information). The correlation coefficients (R^2) are in the range of 0.98−0.99, and the maximum adsorption capacity is 416, 125, and 318 mg/g for MPTMS-biomagnetite, biomagnetite, and XUS, respectively. The good agreement between the data and the Langmuir adsorption model indicates that the extent of mercury adsorption is a function of specific binding sites, a finite number of which are located on the sorbent surface. The isotherm results further suggest that the large number of accessible −SH ligands on the biomagnetite surface led to the large mercury sorption capacity, which is higher than that of XUS, a Hg(II)-specific chelating resin. We note that the adsorption of Hg(II) to the container wall was negligible, because of the competition from the sorbents. The extraction of reaction bottles after sorption tests with 1% HCl showed <0.04% and 0.84% of the total Hg were adsorbed to the container walls when XUS and GAC were used as the sorbents, respectively.

Table 2. Leaching of Fe, Zn, Si, and S from 100 mg/L MPTMS-Biomagnetite and Biomagnetite in Different Water Matrix for 6 h

	MPTMS-Biomagnetite				Biomagnetite	
water matrix	% Fe leached per total Fe	% Zn leached per total Zn	% Si leached per total Si	% S leached per total S	% Fe leached per total Fe	% Zn leached per total Zn
DI water	0.04	0.19	0.03	0	0	0.14
Y-12 source water, pH 8.0	0.23	0.21	0.80	N/A	N/A	N/A
Y-12 source water, pH 3.0	0.87	2.02	0.80	N/A	N/A	N/A
0.1 M HNO_3	1.25	6.58	3.60	0	2.89	19.4
0.1 M HCl	1.46	9.38	3.90	0	N/A	N/A
0.5 M HNO_3	2.21	9.36	4.80	0	6.22	21.3
1.0 M HNO_3	4.05	12.0	8.30	1.50	11.0	25.5
5.0 M HNO_3	46.5	58.6	8.80	2.50	67.6	92.6
2.0 M NaOH	0.87	5.01	86.3	60.3	0.40	8.3

It is also interesting that the Hg(II) adsorption isotherm by SAMMS in the YWW solution did not follow the Langmuir model (R^2 = 0.33). It was unexpected that the maximum Hg(II) sorption capacity of SAMMS was lower than that of XUS and MPTMS-biomagnetite, since it has higher binding affinity K_d for Hg(II) in YWW solution. The capacity of SAMMS for Hg(II) in DI water was reported to be as high as 613 mg/g.[25] The measured Hg(II) capacity in YWW reported here is only ~176 mg/g (from Langmuir fitting), which may indicate poor utilization of the inner SAMMS binding sites in YWW at high mercury concentration. (Note that the high K_d for Hg(II) of SAMMS was measured at Hg(II) concentration of 0.12 μM.) Yantasee et al.[31]reported a similar Hg(II) sorption capacity for SAMMS (167 mg/g) and a very low capacity (8 mg/g) for a thiol-based resin (GT-73) in a groundwater sample (pH 8.1). Therefore, the wastewater characteristics is an important factor affecting the overall performance of the sorbents. For Y-12 wastewater, MPTMS-biomagnetite has an overall best performance among all the commercial Hg(II) sorbents evaluated, because of its higher Hg(II) sorption capacity and faster sorption kinetics. Table 1 also summarizes the important features of reported magnetic nanostructured mercury sorbents and their Hg(II) uptake performance. It is clear that MPTMS-biomagnetite has the highest capacity for Hg(II) removal, even when tested in industrial wastewater. At maximum sorption, the molar ratio of Hg(II) per thiol was ~0.58:1, suggesting that the −SH groups on MPTMS were fully utilized with one Hg bonding to two −SH groups. The full utilization of thiol groups by Hg(II) also demonstrates high selectivity of MPTMS-biomagnetite for Hg(II) over other metal ions present in Y-12 wastewater.

Stability of the Nanomaterial. Table 2 shows the extent of the Fe, Zn, Si, and S leaching into the solution phase after contact between both biomagnetite and MPTMS-biomagnetite and various fluids for 6 h. In matrices ranging from 1 M acid to a strong alkaline solution (2.0 M NaOH), <12 wt % of total Fe and Zn leached from the MPTMS-biomagnetite, suggesting that these sorbents are relatively stable and can be used in most natural and wastewaters (pH 4−8). The low leaching of Fe from MPTMS-biomagnetite also minimizes the loss of its magnetic recoverability. In contrast, significantly higher (2−3 times) amounts of Fe and Zn were found in the leachate of biomagnetite. Therefore, the MPTMS coating on the surface of the biomagnetite, with a thickness of ~5 nm, played an important role in protecting the biomagnetite core from attack by acids and bases especially acids. Further increasing the acid concentration to 5 M significantly increased the dissolution of Fe and Zn but not of Si and S (<9%), demonstrating that the MPTMS coating is more stable than the exposed biomagnetite core, and the dissolution of the core did not result in the concurrent detachment of the coating from the core. As expected, the Si−O bonds are unstable under strong-base conditions. About 86.3% and 60.3% of Si and S leached out in 2.0 M NaOH, respectively. However, the leaching content of Fe and Zn was <5%, which showed that the MPTMS coating detached from the core as a result of the breakdown of Si−O bonds at high pH. For either biomagnetite or MPTMS-biomagnetite, the leaching of Zn is apparently faster than that of Fe under the same condition, suggesting that Zn is more labile and leaches out in environmental media. This finding can be explained by the paragenetic sequence of biomagnetite as the mineral transforms directly or indirectly—by initially forming maghemite (γ-Fe_2O_3)—to hematite (α-Fe_2O_3) resulting in the liberation of Fe(II) and Zn(II) from the structure.[57,58] It is important to note that Fe(II) is probably oxidized in solution to Fe(III) and incorporated into the biomagnetite, whereas Zn(II), which has been substituted for Fe(II) in the Zn-doped biomagnetite structure, remains in solution after being released. Structure, charge distribution, and electron hopping dynamics determine the rate and extent of the interfacial redox reactions that control the oxidative transformation process that releases Zn from biomagnetite.[59] However, in environmentally relevant water media (pH 4−8), the leaching of all four elements (Fe, Zn, Si, and S) should be minimal.

■ ASSOCIATED CONTENT

Supporting Information

Additional data on biomagnetite synthesis, major water chemistry of filtered YWW, Freundlich isotherm modeling, and schematic details regarding formation of MPTMS layers on biomagnetite surface. This material is available free of charge via the Internet at http://pubs.acs.org.

■ AUTHOR INFORMATION

Corresponding Author

*Tel.: (865) 574-5278. Fax: (865) 576-8646. E-mail: hef2@ornl.gov.

Notes

The authors declare no competing financial interest.

■ ACKNOWLEDGMENTS

This research was supported by the Office of Groundwater and Soil Remediation, Office of Environmental Management, U.S. Department of Energy (DOE) as part of the Applied Field Research Initiative (AFRI) Program at Oak Ridge National Laboratory (ORNL), which is managed by UT-Battelle LLC for the DOE under Contract No. DE-AC05-00OR22725. STEM work was sponsored by Oak Ridge National Laboratory's Shared Research Equipment (ShaRE) User Program, which is sponsored by the Office of Basic Energy Sciences, U.S. DOE.

■ REFERENCES

(1) Gu, B. H.; Bian, Y. R.; Miller, C. L.; Dong, W. M.; Jiang, X.; Liang, L. Y. *Proc. Natl. Acad. Sci. U. S. A.* **2011**, *108*, 1479−1483.
(2) Morel, F. M. M.; Kraepiel, A. M. L.; Amyot, M. *Annu. Rev. Ecol. Syst.* **1998**, *29*, 543−566.
(3) Harris, H. H.; Pickering, I. J.; George, G. N. *Science* **2003**, *301*, 1203−1203.
(4) United States Environmental Protection Agency (EPA). *Treatment technologies for mercury in soil, waste, and water*; EPA Report EPA-542-R-07-003, U.S. EPA: Washington, DC, 2007.
(5) Tonini, D. R.; Gauvin, D. A.; Soffel, R. W.; Freeman, W. P. *Environ. Prog.* **2003**, *22*, 167−173.
(6) Huang, C. P.; Blankenship, D. W. *Water Res.* **1984**, *18*, 37−46.
(7) Lloyd-Jones, P. J.; Rangel-Mendez, J. R.; Streat, M. *Process Saf. Environ. Prot.* **2004**, *82*, 301−311.
(8) Miretzky, P.; Cirelli, A. F. *J. Hazard. Mater.* **2009**, *167*, 10−23.
(9) Shafaei, A.; Ashtiani, F. Z.; Kaghazchi, T. *Chem. Eng. J.* **2007**, *133*, 311−316.
(10) Blanchard, G.; Maunaye, M.; Martin, G. *Water Res.* **1984**, *18*, 1501−1507.
(11) Benhammou, A.; Yaacoubi, A.; Nibou, L.; Tanouti, B. *J. Colloid Interface Sci.* **2005**, *282*, 320−326.
(12) Viraraghavan, T.; Kapoor, A. *J. Environ. Sci. Health, Part A: Toxic/Hazard. Subst. Environ. Eng.* **1995**, *30*, 553−566.
(13) Fernandez-Nava, Y.; Ulmanu, M.; Anger, I.; Maranon, E.; Castrillon, L. *Water, Air, Soil Pollut.* **2011**, *215*, 239−249.
(14) Hovsepyan, A.; Bonzongo, J. C. J. *J. Hazard. Mater.* **2009**, *164*, 73−80.
(15) Lagadic, I. L.; Mitchell, M. K.; Payne, B. D. *Environ. Sci. Technol.* **2001**, *35*, 984−990.
(16) Tchinda, A. J.; Ngameni, E.; Kenfack, I. T.; Walcarius, A. *Chem. Mater.* **2009**, *21*, 4111−4121.
(17) Mercier, L.; Pinnavaia, T. J. *Microporous Mesoporous Mater.* **1998**, *20*, 101−106.
(18) Chiarle, S.; Ratto, M.; Rovatti, M. *Water Res.* **2000**, *34*, 2971−2978.
(19) Nam, K. H.; Gomez-Salazar, S.; Tavlarides, L. L. *Ind. Eng. Chem. Res.* **2003**, *42*, 1955−1964.
(20) Nam, K. H.; Tavlarides, L. L. *Solvent Extr. Ion Exch.* **2003**, *21*, 899−913.
(21) Brown, J.; Mercier, L.; Pinnavaia, T. J. *Chem. Commun.* **1999**, 69−70.
(22) Mercier, L.; Pinnavaia, T. J. *Adv. Mater.* **1997**, *9*, 500−503.
(23) Mercier, L.; Pinnavaia, T. J. *Environ. Sci. Technol.* **1998**, *32*, 2749−2754.
(24) Mercier, L.; Pinnavaia, T. J. In *Natural Microporous Materials in Environmental Technology*; Misaelides, P., Macasek, F., Pinnavaia, T. J., Colella, C., Eds.; Kluwer Academic Publishers: Dordrecht, The Netherlands, 1999; Vol. *362*, p 33.
(25) Chen, X. B.; Feng, X. D.; Liu, J.; Fryxell, G. E.; Gong, M. L. *Sep. Sci. Technol.* **1999**, *34*, 1121−1132.
(26) Feng, X.; Fryxell, G. E.; Wang, L. Q.; Kim, A. Y.; Liu, J.; Kemner, K. M. *Science* **1997**, *276*, 923−926.
(27) Mattigod, S. V.; Feng, X. D.; Fryxell, G. E.; Liu, J.; Gong, M. L. *Sep. Sci. Technol.* **1999**, *34*, 2329−2345.
(28) Walcarius, A.; Delacote, C. *Anal. Chim. Acta* **2005**, *547*, 3−13.
(29) Shin, Y. S.; Fryxell, G.; Um, W. Y.; Parker, K.; Mattigod, S. V.; Skaggs, R. *Adv. Funct. Mater.* **2007**, *17*, 2897−2901.
(30) Stumm, W., Morgan, J. J. *Aquatic Chemistry*; Wiley−Interscience: New York, 1995.
(31) Yantasee, W.; Warner, C. L.; Sangvanich, T.; Addleman, R. S.; Carter, T. G.; Wiacek, R. J.; Fryxell, G. E.; Timchalk, C.; Warner, M. G. *Environ. Sci. Technol.* **2007**, *41*, 5114−5119.
(32) Hu, J.; Chen, G. H.; Lo, I. M. C. *Water Res.* **2005**, *39*, 4528−4536.
(33) Mayo, J. T.; Yavuz, C.; Yean, S.; Cong, L.; Shipley, H.; Yu, W.; Falkner, J.; Kan, A.; Tomson, M.; Colvin, V. L. *Sci. Technol. Adv. Mater.* **2007**, *8*, 71−75.
(34) Yavuz, C. T.; Mayo, J. T.; Yu, W. W.; Prakash, A.; Falkner, J. C.; Yean, S.; Cong, L. L.; Shipley, H. J.; Kan, A.; Tomson, M.; Natelson, D.; Colvin, V. L. *Science* **2006**, *314*, 964−967.
(35) White, B. R.; Stackhouse, B. T.; Holcombe, J. A. *J. Hazard. Mater.* **2009**, *161*, 848−853.
(36) Chang, Y. C.; Chen, D. H. *J. Colloid Interface Sci.* **2005**, *283*, 446−451.
(37) Zhou, Y. T.; Nie, H. L.; Branford-White, C.; He, Z. Y.; Zhu, L. M. *J. Colloid Interface Sci.* **2009**, *330*, 29−37.
(38) Jiang, Y. J.; Li, X. T.; Gao, J.; Guo, X. C.; Guan, J.; Mu, X. D. *J. Nanopart. Res.* **2011**, *13*, 939−945.
(39) Liu, J. F.; Zhao, Z. S.; Jiang, G. B. *Environ. Sci. Technol.* **2008**, *42*, 6949−6954.
(40) Shin, S.; Jang, J. *Chem. Commun.* **2007**, 4230−4232.
(41) Zhai, Y. H.; Duan, S. E.; He, Q.; Yang, X. H.; Han, Q. *Microchim. Acta* **2010**, *169*, 353−360.
(42) Tri, P. M.; Khim, K. S.; Hidajat, K.; Uddin, M. S. *J. Nanosci. Nanotechnol.* **2009**, *9*, 905−908.
(43) Song, B. Y.; Eom, Y.; Lee, T. G. *Appl. Surf. Sci.* **2011**, *257*, 4754−4759.
(44) Liu, J. S.; Du, X. Z. *J. Mater. Chem.* **2011**, *21*, 6981−6987.
(45) Guo, L. M.; Li, J. T.; Zhang, L. X.; Li, J. B.; Li, Y. S.; Yu, C. C.; Shi, J. L.; Ruan, M. L.; Feng, J. W. *J. Mater. Chem.* **2008**, *18*, 2733−2738.
(46) Moon, J. W.; Rawn, C. J.; Rondinone, A. J.; Wang, W.; Vali, H.; Yeary, L. W.; Love, L. J.; Kirkham, M. J.; Gu, B. H.; Phelps, T. J. *J. Nanosci. Nanotechnol.* **2010**, *10*, 8298−8306.
(47) Moon, J. W.; Roh, Y.; Lauf, R. J.; Vali, H.; Yeary, L. W.; Phelps, T. J. *J. Microbiol. Methods* **2007**, *70*, 150−158.
(48) Moon, J. W.; Yeary, L. W.; Rondinone, A. J.; Rawn, C. J.; Kirkham, M. J.; Roh, Y.; Love, L. J.; Phelps, T. J. *J. Magn. Magn. Mater.* **2007**, *313*, 283−292.
(49) Wilson, A. J. C. *Proc. Phys. Soc. London* **1962**, *80*, 286−.
(50) Butler, R. F.; Banerjee, S. K. *J. Geophys. Res.* **1975**, *80*, 4049−4058.
(51) Yeary, L. W.; Moon, J. W.; Love, L. J.; Thompson, J. R.; Rawn, C. J.; Phelps, T. J. *IEEE Trans. Magn.* **2005**, *41*, 4384−4389.
(52) Shen, X. C.; Fang, X. Z.; Zhou, Y. H.; Liang, H. *Chem. Lett.* **2004**, *33*, 1468−1469.
(53) Yamaura, M.; Camilo, R. L.; Sampaio, L. C.; Macedo, M. A.; Nakamura, M.; Toma, H. E. *J. Magn. Magn. Mater.* **2004**, *279*, 210−217.
(54) Yang, S. R.; Kolbesen, B. O. *Appl. Surf. Sci.* **2008**, *255*, 1726−1735.
(55) Hu, M. H.; Noda, S.; Okubo, T.; Yamaguchi, Y.; Komiyama, H. *Appl. Surf. Sci.* **2001**, *181*, 307−316.
(56) Warner, C. L.; Addleman, R. S.; Cinson, A. D.; Droubay, T. C.; Engelhard, M. H.; Nash, M. A.; Yantasee, W.; Warner, M. G. *ChemSusChem* **2010**, *3*, 749−757.
(57) Colombo, U.; Fagheraz., G; Gazzarri., F; Lanzavec., G; Sironi, G. *Nature* **1968**, *219*, 1036−.
(58) Sidhu, P. S. *Clays Clay Miner.* **1988**, *36*, 31−38.
(59) Skomurski, F. N.; Kerisit, S.; Rosso, K. M. *Geochim. Cosmochim. Acta* **2010**, *74*, 4234−4248.